Applied Catalysis B: Environmental 154–155 (2014) 360–368

Contents lists available at ScienceDirect

Applied Catalysis B: Environmental

journal homepage: www.elsevier.com/locate/apcatb

Electrocatalytic selective oxidation of glycerol to tartronate on Au/C anode catalysts in anion exchange membrane fuel cells with electricity cogeneration

Ji Qi[a,1], Le Xin[a,1], David J. Chadderdon[a], Yang Qiu[a], Yibo Jiang[b], Neeva Benipal[a], Changhai Liang[c], Wenzhen Li[a,*]

[a] Department of Chemical Engineering, Michigan Technological University, Houghton, MI, 49931, USA
[b] Department of Civil & Environmental Engineering, Michigan Technological University, Houghton, MI, 49931, USA
[c] School of Chemical Engineering, Dalian University of Technology, Dalian, Liaoning, China

ARTICLE INFO

Article history:
Received 29 October 2013
Received in revised form 22 January 2014
Accepted 14 February 2014
Available online 28 February 2014

Keywords:
Selective oxidation
Glycerol
Gold nanoparticles
Fuel cell
Cogeneration

ABSTRACT

Sustainable cogeneration of tartronate (high yield of 61.8%) and electrical energy (1527 J, 12 h) has been achieved from direct electrocatalytic oxidation of glycerol on Au/C in a 5 cm^2 anion exchange membrane-direct glycerol fuel cells (AEM-DGFCs). The electrode structure and reaction conditions exhibited strong effects on the anode potential, which can be tuned to <0.45 V in favor of oxidizing two primary —OH groups of glycerol while minimizing over-oxidation of the secondary —OH and C—C bond cleavage, thereby promoting the tartronate production. The relatively low activity of partial oxidation products (glycerate, tartronate, mesoxalate) on Au/C revealed in half cell indicates that the tartronate generation in AEM-DGFCs is through direct adsorbed C_3 intermediates oxidation. Mass transport of reactants and reaction intermediates governed by the operational conditions was also found to play a critical role in regulating reaction rate and the desired products selectivity. Furthermore, Au/C prepared via aqueous phase reduction method (Au/C-AQ) was compared with organic phase nanocapsule method (Au/C-NC), and it shows the residual surfactants have little effect on the tartronate yield.

1. Introduction

Non-renewable petroleum nowadays remains the main source for manufacturing of fuels and chemicals in industries, and has been serving for boosting our fast human society growth for decades. However, with the rapid increasing of the global population and continuing improvement of the people's living standards, our heavy addiction to petroleum has aroused great concerns, mainly due to the dwindling of petroleum reserves resulting in the rising cost of the transportation fuels, and more importantly, the air quality deterioration and global climate change [1,2]. Under such situation, it is imperative to search for alternative, renewable natural resources for the fine chemicals production. Glycerol is a key biomass-derived compound, readily available from the bio-diesel manufacture [3]. Due to its three hydroxyl (—OH) groups, glycerol has been recognized as a viable feedstock for the production of a wide range of value-added chemicals [4]. Among them, tartronic acid (TA, a C_3 diacarboxylic acid, product of two primary —OH oxidation of glycerol) has found its medical application in the treatment of osteoporosis and obesity. However, the current high price of TA ($1536 g^{-1}) impedes the expansion of its potential market [5].

Aqueous phase selective oxidation of glycerol to valuable chemicals (including TA) over metal catalysts with molecular oxygen or H_2O_2 oxidant represents a very attractive green process due to its low environmental impact, especially when compared to current stoichiometric oxidation processes. Although great progress has been made on selective oxidation of one primary —OH group of glycerol to glycerate over Pt, Pd, Au catalysts, it is still challenging to selectively oxidize two primary —OH groups to generate tartronate on monometallic catalysts. Prior studies were primary focused on enhancing the activity and selectivity to glycerate of Pt, Pd and Au-based mono-[6–13] and bi-metallic [10,11,14–16] catalysts, however under certain reaction conditions, the selectivity to di-carboxylic acid (e.g. tartronate) via consecutive oxidation of glycerol was found to be promoted. Prati and Hutchings groups have demonstrated that increasing the catalyst amount and decreasing the glycerol concentration can promote the tartronate

* Corresponding author. Tel.: +1 906 487 2298; fax: +1 906 487 3213.
E-mail addresses: wzli@mtu.edu, liwenzhen@gmail.com (W. Li).
[1] These authors contributed equally to this work.

http://dx.doi.org/10.1016/j.apcatb.2014.02.040
0926-3373/

formation, which could be attributed to the increasing of the ratio of glycerol to catalyst active sites [7,16,17]. It was also observed that by increasing the reaction temperature and oxygen concentration, the transformation of glycerate to tartronate could be facilitated [7,8]. Independent studies by Prati and Davis have reported that glycerol oxidation carried out in a fixed bed continuous up-flow reactor significantly increased the selectivity to tartronate compared with that conducted in semi-batch reactor [18,19]. Even though research breakthrough has been made to obtain reasonable yield of tartronate, complicate multi-metallic catalysts (0.8%Ce-1.5%Bi-0.75%Pt-3%Pd/C [20] and 0.1% Bi@AuPd/AC [21]) have to be used. More importantly, conventional heterogeneous catalytic oxidation of glycerol that takes place in aqueous phase with O_2 or H_2O_2 oxidant cannot take advantage of the rich energy stored in the chemical bonds of glycerol, which can be directly converted to electrical energy via electrochemical oxidation.

Exhaustive research efforts in electrochemical oxidation of glycerol have been made aiming to gain fundamental understanding of the key factors that govern the electrocatalytic oxidations. In situ Fourier transform infrared (FTIR) spectroscopy and high performance liquid chromatograph (HPLC) combined with voltammetry have been applied to probe reaction intermediates/products under a wide range of potentials in half cells [22–29]. HPLC has identified that glycerate and glycolate are two dominant products on monometallic Pt, Pd and Au in alkaline electrolyte. Tartronate was observed as a small amount side product only on Au/C and both polycrystalline bulk Pt electrode and Pt/C at low potentials, whereas on polycrystalline bulk Au electrode, the presence of tartronate was detected as a weak FTIR signal at very high potentials of >1.2 V vs. RHE (reversible hydrogen electrode). In addition, Simoes et al. performed the electro-oxidation of glycerol on bimetallic PdAu, PdNi, PdBi and trimetallic PdPtBi nanoparticle catalysts [24,30]. With the assistance of spectroscopy or chromatography analysis, it was proposed that the activity of glycerol electro-oxidation could be promoted by ad-atoms and the formation of tartronate is strongly dependent on the electrode potential.

Direct glycerol fuel cells (DGFCs) have attached enormous attention as a potential mobile electrochemical power source for transportations and portable electronics. Pt-,Pd- and Au- based anode catalysts have been investigated in DGFCs with solid anion exchange membrane electrolyte [27,31–39]. Although tremendous progress in the electrical energy generation performance have been accomplished through rational design of electrocatalyst structures, complete oxidation of glycerol to carbonate in alkaline media remains the minor reaction in comparison with its partial oxidation to various carboxylates [40], which will lead to low energy density and utilization efficiency of glycerol fuel. For this reason, DGFCs may have industrial application potential only if reasonable output power density and high yield of higher-valued target products can be achieved simultaneously [37,41]. Early work in our lab has successfully achieved the cogeneration of electricity (58.6 mW cm^{-2} on Pt/C and 22.7 mW cm^{-2} on Au/C) and valuable chemicals (selectivity of 41% to glycerate + 50% tartronate on Pt/C and 46% to mesoxalate on Au/C) in anion exchange membrane-direct glycerol fuel cells (AEM-DGFCs) [27,42]. Recently Vizza et al. conducted electro-oxidation of glycerol in passive AEM-DGFCs and reported selectivity of 55.3% and 43.4% to glycerate and tartronate, with electrical energy generation of 578 and 366 J on Pd-(Ni-Zn)/C and Pd/C, respectively [33,40]. Ilie et al. has reported that the fuel cell operating conditions such as anode fuel rate has an effect on the cell potential in direct glycerol fuel cell [43]. Very recently, AEM-based electrolysis flow cell reactor was self-designed by our group and used to investigate glycerol electro-oxidation on Au/C with carbon cloth substrate (liquid diffusion layer), this is similar to AEM-DGFC anode structures. It is interesting to find that the degree of glycerol oxidation can be well tuned by anode potential to produce tartronate (oxidizing two primary —OH) at <0.45 V vs. RHE, mesoxalate (oxidizing three —OH) at ≥0.45 V vs. RHE, or glycolate (breaking C—C bond) at >0.9 V vs. RHE [28,44]. Therefore, it would be very attractive to seek co-production of valuable tartronate and electricity over Au/C catalysts in AEM-DGFC, if we could lower the anode potential to <0.45 V, as what we have discovered in electrolysis cell study.

Herein, we report cogeneration of electricity and tartronate with a high yield of 61.8% from direct glycerol oxidation on Au/C anode catalysts in AEM-DGFC. The optimization of membrane electrode assembly (MEA) structure, electrolyte pH, fuel flow rate and operation temperature were found to allow fine tuning of the anode potential to fairly low of <0.45 V in order to favor the electro-oxidation of two primary —OH groups of glycerol (to tartronate), while minimizing over-oxidation of the secondary —OH (to mesoxalate) and the C—C bond cleavage (e.g. to glycolate and oxalate). It is also found that in AEMFC Au/C catalyzed glycerol partial oxidation products (glycerate, tartronate, mesoxalate) are relatively stable after desorbing into bulk electrolyte, which has been further supported by half-cell experiment. For comparative purpose, Au/C anode catalysts prepared by both organic phase nanocapsule method (Au/C-NC) and aqueous phase reduction method (Au/C-AQ) were studied for electrocatalytic select oxidation of glycerol in AEM-DGFCs and it is shown that the surfactants involved in the Au/C-NC synthesis has little effect on the final oxidation products distribution.

2. Experimental

2.1. Chemicals

$AuCl_3$ was purchased from Alfa Aesar. Sodium borohydride (99%), sodium citrate dihydrate (99%), $LiBEt_3H$ (1 M in THF), 1-octadecene (90%), and benzyl ether (99%) were purchased from Acros Organics. Carbon support (Vulcan XC72R) was obtained from Fuel Cell Store. Polytetrafluoroethylene (PTFE), oleylamine (70%), potassium sulfate (99%), 1-propanol (99.5%) and most of the standard samples including D-glyceric acid calcium salt dehydrate (99%), sodium mesoxalate monohydrate (98%) oxalic acid (99%), glycolic acid (99%), lactic acid (90%), formic acid (98%) were bought from Sigma–Aldrich. Oleic acid (90%) and high purity glycerol (99.8%) were purchased from Fisher Scientific. All the chemicals were used as received without further purification.

2.2. Preparation of Au/C catalysts

Au/C prepared by organic phase nanocapsule method (Au/C-NC): $AuCl_3$ (151.7 mg) was dissolved in a mixture of 1-octadecene (16 mL) and oleylamine (4 mL) under a nitrogen blanket. The system was then heated to 80 °C, followed by a quick injection of $LiBEt_3H$ (1.5 mL). After holding the temperature constant for 10 min, the solution was cooled down to room temperature and the Au nanoparticles (NPs) were separated by 10,000 rpm centrifugation for 10 min. The as-prepared Au NPs were re-dispersed in hexane (50 ml) and dropped at a rate of 1 s^{-1} into carbon black (80.6 mg or 147.7 mg) dispersed in ethanol. The as-prepared Au NPs were re-dispersed in hexane (50 ml) and slowly dropped into an ethanol dispersion of carbon black (80.6 mg or 147.7 mg). The final product Au/C-NC catalyst with a loading of 55 wt% or 40 wt% was obtained after filtration, washed with ethanol (1 L) and dried in the vacuum oven at 50 °C overnight.

Au/C prepared by aqueous phase method (Au/C-AQ): The catalyst precursor, $AuCl_3$ (151.7 mg), was dissolved in DI water (1500 mL) by 5 min ultrasonic sonication. The catalyst support, 80.6 mg of carbon black, was ultra-sonicated and stirred for 10 min

to form a homogeneous ink. Citrate-stabilized reducing agent solution was prepared by dissolving sodium citrate dihydrate (200 mg) and sodium borohydride (60 mg) in DI water (50 mL) and was then added to the $AuCl_3$ solution under vigorous stirring. Subsequently, the carbon black ink was mixed with the as-prepared Au hydrosol. In order to facilitate the deposition of Au NPs onto the carbon support, 0.4 M potassium sulfate solution (150 mL) was slowly pumped into the aforementioned mixture in 12 h. After filtrated and dried in the vacuum oven at room temperature overnight, Au/C-AQ catalyst with a loading of 55 wt% was obtained.

2.3. Physical characterization of Au/C catalysts

The structure, composition and morphology of Au/C catalysts were characterized by X-ray diffraction (XRD), and transmission election microscopy (TEM). Scintag XDS-2000 θ/θ diffractometer (Cu Kα radiation (λ = 1.5406 Å) with 35 mA filament current and 45 kV tube voltage) were employed to collect XRD patterns at a continuous scan rate of 1.2 degree per minute. The mean crystallite sizes of Au/C-NC and Au/C-AQ catalysts are calculated using the (2 2 0) peak based on Debye–Scherrer formula:

$$L = \frac{0.9\lambda_{K\alpha}}{B_{2\theta}\cos\theta_{\max}} \quad (1)$$

where L is the mean crystal size, λ is the wavelength of the X-ray (1.5406 Å), B is the full width at half-maximum of the peak (rad) and $\theta_{\max}$ is the Bragg angle (rad) of Au (2 2 0).

The transmission electron microscopy (TEM) image of Au/C was collected on JEOL JEM-4000FX with an operating voltage of 200 kV.

2.4. Membrane electrode assembly (MEA) fabrication

The anode catalyst ink was made by mixing Au/C catalyst power, 5 wt% PTFE in water suspension into iso-propanol (10 $mg_{catalyst}$/ml, mass ratio PTFE:catalyst = 5:95), and sprayed onto a carbon cloth (PTFE-untreated, 381 μm, Fuel Cell Store) that serves as the liquid diffusion layers (LDL) to achieve a loading of 1.0 mg_{Au} cm^{-2}. The cathode catalyst ink (10 $mg_{catalyst}$/ml, mass ratio ionomer:catalyst = 3:7), which was made from 1-propanol dispersion of a commercial non-precious metal HYPERMECTM (Fe-Cu-based catalyst, Acta 4020) blended with an AS-4 anon conductive ionomer (Tokuyama), was airbrushed directly onto the AEM. Carbon paper (Toray) was employed as the cathode gas diffusion layer. The evenly-sprayed carbon cloth anode and catalyst coated membrane (CCM) cathode were dried in air under room temperature overnight before use. The MEA was fabricated by directly assembling the anode, cathode and carbon paper in sequence without hot press.

2.5. Anion exchange membrane fuel cells (AEM-DGFCs) test and product analysis

Electro-catalytic oxidation of glycerol in AEM-DGFC was conducted on a Scribner fuel-cell test stand (850e). The fuel cell fixture was purchased from Fuel Cell Technology Inc. with an active area of 5 cm^2. The end plate was modified with stainless steel (316L) to tolerate the alkaline operation environment. During each run, 30 ml of glycerol + KOH solution was introduced into a plastic vessel and pumped into the anode at a flow rate of 1.0 or 4.0 ml min^{-1} through a closed loop by a peristaltic pump (Gilson Minipuls 3), while the high-purity O_2 (>99.999%) was fed into the cathode compartment at a flow rate of 0.1 or 0.4 L min^{-1} under a backpressure of 30 or 0 psig. The electro-oxidation was carried out by controlling the fuel cell voltage to 0.1 V. During the reaction, the anode potentials were monitored by a Hg/HgO/1.0 M KOH reference electrode and converted to reversible hydrogen electrode (RHE) by V vs. RHE = V measured vs. Hg/HgO/1.0 M KOH + 0.098 + 0.059 × (pH of electrolyte solution). Hg/HgO/1.0 M KOH reference electrode was calibrated against RHE (HydroFlex®) in a fresh prepared 1.0 M KOH electrolyte at the end of each test, and their potential difference was maintained 0.924 ± 0.007 V in all of the experiments. Samples were removed periodically and analyzed by HPLC using a column (Alltech, OA-1000) with a refractive index detector (RID, Agilent G1362A) and a variable wavelength detector (VWD, 220 nm, Agilent G1314A). An eluent of 5 mM aqueous sulfuric acid at a flow rate of 0.3 ml min^{-1} were applied for the product separation. 20 μl of sample was injected into the HPLC system. Products were identified by comparison with authentic samples.

The product selectivity/yield and glycerol conversion are calculated by the following equations:

$$\text{Selectivity of one } C_2 \text{ or } C_3 \text{ product} = \frac{\text{moles of } C_2 \text{ or } C_3 \text{ product}}{\text{total moles of } C_2 \text{ and } C_3 \text{ products}} \times 100\% \quad (2)$$

$$\text{Conversion of glycerol} = \left(1 - \frac{\text{concentration of glycerol at certain time}}{\text{Initial concentration of glycerol}}\right) \times 100\% \quad (3)$$

$$\text{Yield of } C_2 \text{or } C_3 \text{ product} = \text{selectivity of } C_2 \text{ or } C_3 \text{ product} \times \text{conversion of glycerol} \quad (4)$$

The carbon balance is based on [19,45]:

$$\text{Carbon balance} = \frac{3M_{gi} - 3\sum M_{C3} - 2\sum M_{C2} - 1\sum M_{C3} - 3\sum M_{gf}}{3M_{gi}} \times 100\% \quad (5)$$

where M_{gi} and $\sum M_{gf}$ is the initial and final moles of glycerol in the electrolyte. $\sum M_{C3}$, $\sum M_{C2}$ and $\sum M_{C1}$ is the total moles of C_3 (glycerate, tartronate, mesoxalate, lactate), C_2 (glycolate, oxalate, glyoxylate) and C_1 (formate, carbonate) products, respectively.

If assuming that no C—C bond cleavage occurs in C_2 products, then $\sum M_{C2} = \sum M_{C1}$. Thus the equation for carbon balance calculation can be simplified to:

$$\text{Carbon balance} = \frac{M_{gi} - \sum M_{C3} - \sum M_{C2} - \sum M_{gr}}{M_{gi}} \times 100\% \quad (6)$$

Therefore, a carbon balance of 0 means all the C_2 products generated from C—C breaking of C_3 products do not undergo further C—C cleavage, and the summation of all the C_2 and C_3 products and unreacted glycerol is equal to the initial glycerol. A smaller carbon balance value indicates less C_2 intermediates were further oxidized to C_1 products (carbon balance of 0 means no C_2 intermediates were further oxidized to C_1 products). The carbon balance under all the tests condition is less than 15%, which is within the system error expected in HPLC analysis.

2.6. Half cell test

Half cell tests were performed in a conventional three-electrode-cell setup, equipped with a glassy carbon working electrode, a Hg/Hg (1.0 M KOH) reference electrode and a Pt wire counter electrode. A water bath is used to hold system temperature at 25, 50, or 60 °C throughout the tests. 2.0 mg Au/C (55 wt%) was firstly dispersed in 1.0 ml isopropanol by sonication to form uniform ink. Before each test, 20 μl of the 2.0 mg ml^{-1} catalyst ink was drop-casted on the glass carbon electrode, followed by adding 10 μl

of 0.05 wt% AS-4 anion conductive ionomer (Tokuyama) on the top to bind the catalyst particles. Prior to tests, all the electrolytes were deaerated by purging with N_2 gas (99.99%) for 30 min. Ten cycles of cyclic voltammograms (CVs) were recorded for Au/C catalyst at 25, 50, and 60 °C in 0.1 M KOH and the stabilized polarization curve obtained from the last cycle as reported. All potentials were reported with respect to RHE. A linear sweep voltammetry (LSV) on Au/C catalyst with sweep rate of 1 mV s^{-1} without rotation was carried out in 0.1 M KOH, 0.1 M KOH + 0.1 M glycerol, 0.2 M KOH + 0.1 M glyceric acid, 0.3 M KOH + 0.1 M tartronic acid and 0.1 M KOH + 0.1 M sodium mesoxalate monohydrate at 50 or 60 °C. Excessive KOH (0.2 or 0.3 M) was used to neutralize glyceric acid (pK_a = 3.52) and tartronic acid (pK_a1 = 2.42, pK_a2 = 4.54) [46].

3. Results and discussion

3.1. The effects of MEA structures and reaction conditions on the tartronate selectivity in AEM-DGFC and electro-oxidation activity evaluation of main glycerol partial oxidation C_3 products in half cell

Electrocatalytic oxidation of glycerol in AEM-DGFCs could provide a new route to sustainable conversion of glycerol to value-added oxygenated chemicals with important industrial applications. The AEM-DGFCs can be envisioned as a continuous fixed-bed reactor with multiple plates, which is more prone to produce deeply oxidized products than conventional heterogeneous catalytic oxidation of glycerol in semi-batch reactor configuration [17–19]. In electrocatalysis, the oxidation reactions take place at the electrified catalyst–electrolyte interface close to the anode, where the reaction rate, pathway and products distribution can be regulated via manipulation of the anode potential, so as to facilitate the formation of valuable target products. Considering that glycerol electro-oxidation on Au/C in AEM-DGFCs involves complex reaction sequences, any changes in reaction conditions, such as the electrode thickness, flow rate, the reaction temperature and electrolyte pH, could affect the anode potential, thereby influencing the final products distribution.

Electrode thickness was first optimized toward anode potential tuning for selective oxidation of glycerol in AEM-DGFC. The different anode thicknesses (length scales) result in different time scales of which the reactants diffuse into and products diffuse out of the porous electrodes, which affect the concentration profiles of reactants and reaction intermediates available inside the electrocatalytically active region. In other words, the thicker the porous electrode is, the more reaction intermediates will be held within the confined electrolyte volume to possibly facilitate their deeper oxidation, meanwhile, the fresh reactant will be held outside of the electrocatalytically active region. Increasing the metal loading of Au/C catalyst from 40 wt% to 55 wt% decreases the amount of carbon black amount on the anode (from 7.5 mg to 4.0 mg), therefore decreases the thickness of the porous liquid diffusion anode (from 705 μm to 597 μm, including the thickness of carbon cloth substrate of 381 μm and catalyst layer of 324 μm or 216 μm measured by a micrometre), given that the same Au loading (1.0 mg_{Au} cm^{-2}) was used at the anode. Compared to the Au/C (1.0 mg_{Au} cm^{-2}, 40 wt%) anode used in our previous work [42], the presented thinner porous anode structure (1.0 mg_{Au} cm^{-2}, 55 wt%), allows more fresh glycerol from bulk electrolyte to replenish the oxidation reaction, which leads to the glycerol conversion increasing from 13.1% (Fig. 1(a)) to 14.7% (Fig. 1(b)) in 1 h operation. Higher local concentration of glycerol presented at the catalyst–electrolyte interface will not only negatively shift the onset potential of glycerol electro-oxidation in half cell but also increase the open circuit voltage (OCV) in AEM-DGFC, as it facilitates the formation of highly reactive

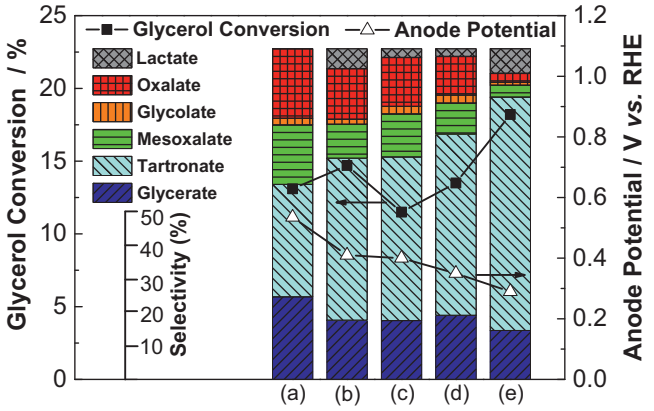

Fig. 1. Electro-catalytic selective oxidation of glycerol in AEM-DGFCs with different MEA structures and operation conditions. Anode catalyst: Au/C-NC; cathode catalyst: Fe-Cu-based catalyst (Acta 4020); anode fuel: 1.0 M glycerol in KOH electrolyte, 30 ml; glycerol:Au = 1:1300 (mol:mol); cell voltage: 0.1 V; reaction time: 1 h. Details of MEA structure and operation conditions (a)–(e) are listed in Table 1.

glyceraldehyde [38,47]. The cathode non-precious Fe-Cu-based catalyst loading was also increased from 1.0 mg/cm^2 to 3.0 mg/cm^2 to facilitate oxygen reduction reaction (ORR). It was observed that the measured anode potential decreases from 0.54 V to 0.41 V vs. RHE with the anode thickness decreasing and enhanced ORR. This observation can also be explained by the ease of the removal of reaction intermediates by glycerol fluxing in through the thinner porous electrode, as their presence could inhibit the oxidation of glycerol [48] and lead to the anode potential increasing. The independent linear scan voltammetry (LSV) experiments were carried out at 50 °C by using KOH solution with glycerate, tartronate, or mesoxalate (Fig. 2(a)). It shows that glycerate is more difficult to be oxidized on Au/C than glycerol as shown by its lower peak current density (e.g.4.5 mA cm^{-2} vs. 23.6 mA cm^{-2} at 50 °C) and more positive onset potential (e.g. 0.82 V vs. ca. 0.57 V (vs. RHE) at 50 °C). It needs even higher onset potentials of about 1.2 and 1.3 V vs. RHE, respectively, for tartronate and mesoxalate adsorption and oxidation on Au/C. This strongly indicates that desorbed glycerate, tartronate and mesoxalate are difficult to be further oxidized under the fuel cell operation conditions (low anode potentials).

As already noted in the previous publications, the C—C cleavage product glycolate is nearly inert on both Au smooth polycrystalline and nanoparticle electrodes [49,50]. Therefore, lowering anode potential and enhancing mass transport using the modified thin electrode structure can promote the tartronate formation by the sequential oxidation of glycerol via adsorbed C_3 reactive intermediates, while minimize its over-oxidation to mesoxalate or C—C bond cleavage by-products (glycolate and oxalate), leading to the tartronate selectivity increasing from 34% (Fig. 1(a)) to 49% (Fig. 1(b)) in 1 h. However, the decreasing of the anode potential weakens the adsorption of glyceraldehyde, a possible unstable byproduct generated at low potential (0.4 V vs. RHE) [26]. The desorbed glyceraldehyde decomposes in the bulk alkaline electrolyte, which is likely responsible for the lactate detected in the final products profile (Fig. 1(b)) [51].

Glycerol fuel flow rate for the AEM-DGFC reactor was also optimized to study its effect on the reaction rate and product distribution of glycerol electro-oxidation. Under similar reaction conditions, the liquid flow rate was decreased from 4 ml min^{-1} to 1 ml min^{-1} and the results are shown in Fig. 1(b) and (c). After slowing down the flow rate of 2.0 M KOH + 1.0 M glycerol, it is observed that the glycerol conversion drops from 14.7% to 11.5%, which could also be attributed to the more intimate contact between the reaction intermediates and catalyst confined within the porous electrode through lowering the fuel flow rate. Although the fuel

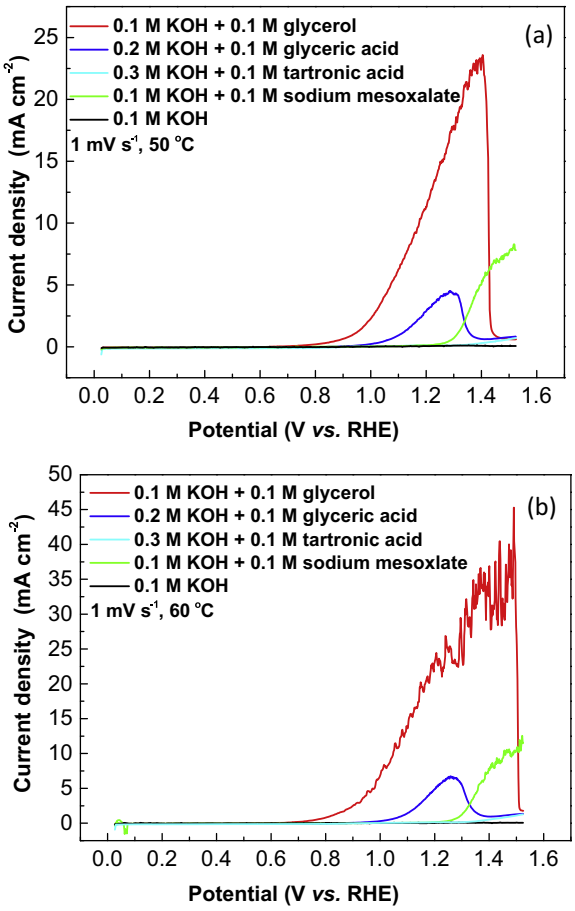

Fig. 2. Linear sweep voltammograms of Au/C-NC (55 wt%) in 0.1 M KOH + 0.1 M glycerol, 0.2 M KOH + 0.1 M glyceric acid, 0.3 M KOH + 0.1 M tartronic acid, 0.1 M KOH + 0.1 M sodium mesoxalate salt and 0.1 M KOH at a scan rate of 1 mV s^{-1}, without rotation, (a) 50 °C, (b) 60 °C.

flow rate has a minor effect on the anode potential, the increasing of the retention time can help hold/trap the reaction intermediates within the porous matrix of the anode, therefore, glyceraldehyde is more likely to remain chemisorbed at the surface and undergoes consequential oxidation to mesoxalate. This is evidenced by the mesoxalate selectivity increasing from 10% to 13% and the selectivity of the glyceraldehyde-degraded by-product lactate decreasing from 6.0% to 2.6%.

In order to gain insight into the influence of reaction temperature on electro-oxidation of glycerol, CV was performed on Au/C (55 wt%) catalyst in blank 0.1 M KOH at 25, 50, and 60 °C. It is shown in Fig. 3 that with the temperature increasing, the onset potential where Au starts to adsorb OH shifts negatively, and within the potential window investigated (<1.65 V vs. RHE), the oxygen evolution reaction (OER) activity on Au/C is negligible at 25, 50, and 60 °C. Early studies suggested that the presence of the sub-monolayer of the adsorbed OH governs the catalytic behavior of Au for alcohol oxidation [49], and there is no glycerol adsorption before the onset potential of Au(OH) formation [52]. Recent DFT results also indicated that the adsorbed OH will significantly lower the activation barrier for both O—H and C—H bond dissociation and enhance the catalytic activity of Au [45]:

$$H_\beta R - OH_\alpha + OH_{ads} \Leftrightarrow H_\beta R - O_{ads} + H_2O \quad (7)$$

$$H_\beta R - OH_\alpha + OH_{ads} \Leftrightarrow R = O_{ads} + H_2O \quad (8)$$

In our previous studies, it is shown that the onset potential of the glycerol electro-oxidation on Au/C in half cell shifts negatively,

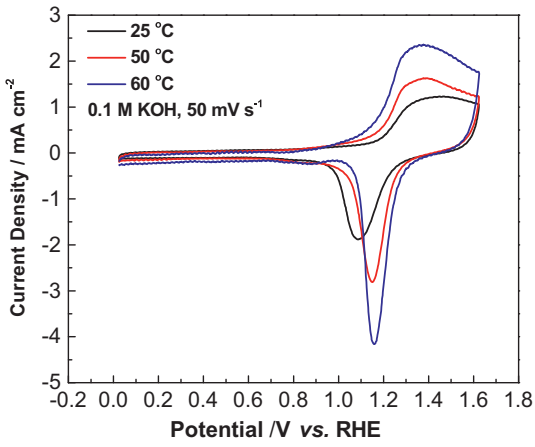

Fig. 3. Cyclic voltammograms of Au/C-NC (55 wt%) in 0.1 M KOH at 25, 50, or 60 °C, at a scan rate of 50 mV s^{-1}, without rotation.

as the reaction temperature increases from 25 °C to 60 °C, which could be attributed to the higher adsorption rate of OH on Au at elevated temperatures [47]. In addition, the reported voltammograms also indicated better electro-oxidation kinetics was achieved at higher temperatures, as shown by the increasing of the peak current density. In agreement with these prior results, it is observed that the AEM-DGFCs operated at higher temperature (60 °C) promotes the glycerol conversion from 11.5% (Fig. 1(c), 50 °C) to 13.5% (Fig. 1(d), 60 °C) in 1 h. Moreover, it further decreases the anode potential from 0.40 V to 0.35 V vs. RHE, contributing to the increasing of tartronate selectivity to 54.8%. On the other hand, the elevated reaction temperature may also promote the reaction intermediates diffusion to the bulk electrolyte, which prevents the further oxidation to mesoxalate, leading to mesoxalate selectivity drop from 13.0% to 9.4%. The by-product lactate selectivity remains small (2.3%), mainly due to the rapid oxidation of glycerol to glycerate via glyceraldehyde at the higher temperature.

High pH alkaline environment has been reported to effectively improve glycerol electro-oxidation rate [27,38,44,53,54]. The AEM-DGFCs fed with 8.0 M KOH + 1.0 M glycerol shows appreciably increasing of the tartronate selectivity from 54.8% to 70.6% and the glycerol conversion from 13.5% to 18.2% when compared to 2.0 M KOH + 1.0 M glycerol (Fig. 1(e)). Higher OH^- concentration was reported to benefit the initial base-catalyzed dehydrogenation of alcohol to promote the generation of highly reactive alkoxy intermediate by lowering the activation barrier [51]:

$$H_\beta R - OH_\alpha + OH^- \Leftrightarrow H_\beta R - O^- + H_2O \Leftrightarrow H_\beta R - O_{ads} + e^- \quad (9)$$

On the other hand, higher OH^- concentration in the bulk electrolyte will increase OH_{ads} coverage rate on Au surface. As aforementioned, the OH_{ads} will also facilitate the elimination of both H_α and H_β of adsorbed alcohols through the metal surface catalyzed process (Eqs. (7) and (8)). As a result, the electrolyte with higher pH (8.0 M KOH + 1.0 M glycerol) greatly enhances the reaction rate, giving rise to the observed higher glycerol conversion and lower anode potential (0.29 V vs. RHE). This result can be supported by our previous studies of electro-oxidation of glycerol over Au/C in half cell, which showed that the onset potential of glycerol oxidation shifted negatively with the KOH concentration increasing [38]. The very low anode potential favors the tartronate formation with a selectivity of 70.6% determined by HPLC analysis. A slight increase of lactate could be also attributed to this low anode potential achieved, as it weakens the adsorption of glyceraldehyde on the Au catalyst. Additionally, the increment of OH_{ads} on Au surface promotes the removal of adsorbed C_3 intermediate species [24,53] to form glycerate or tartronate, before they undergo further oxidation

to mesoxalate or C—C bond breaking to by-products of glycolate and oxalate.

Tartronate has significant market potential. A very high tartronate selectivity of 70.6% from direct glycerol electrooxidation has been achieved in the AEM-DGFC reactor through fine tuning of anode potential, via optimizing the electrode structure and reaction conditions. It is worthy to note that the optimization of mass transfer of the reactant, intermediates and products by varying these operation conditions also plays a critical role in regulating the reaction rate and pathway to the desired products.

3.2. Cogeneration of electricity and tartronate with high yield in AEM-DGFC

Compared with the traditional heterogeneous catalysis, electrocatalytic selective oxidation of glycerol in the AEM-DGFC reactor is a more sustainable process, in which the valuable chemicals and electrical energy can be simultaneously generated [27,42]. As tartronate finds its values in the pharmaceuticals [55], food industries [56–58] and anti-corrosive protective agents [59], we focused our efforts on employing the optimum conditions, as listed in Table 1(e) demonstrating the highest activity and selectivity to tartronate, so as to achieve the high yield of tartronate for potential industrial synthesis applications.

The reaction profile shown in Fig. 4 exhibits that electrocatalytic selective oxidation of glycerol can achieve a tartronate yield of 61.8% (69.3% of selectivity at 89.2% glycerol conversion) after 12 h, concurrently with energy release of 1527 J in the AEM-DGFC reactor with Au/C-NC under the optimized conditions. The maximum yields of tartronate from heterogeneous catalytic oxidation of glycerol have been reported to be 58% on Ce-Bi-Pd-Pt/C [20] and 78% on Bi@AuPd/C [21]. However, mono-Au or AuPd, AuPt heterogeneous catalysts were found to be rather inefficient for tartronate production from direct glycerol oxidation [5]. The high tartronate yield on Au/C electrocatalyst achieved in this work may open an alternative route to sustainable electrocatalytic conversion of biorenewable intermediates to chemicals along with electricity cogeneration.

Table 1
Details of MEA structure and AEM-DGFC operation conditions.

Entry	(a)[a]	(b)	(c)	(d)	(e)
Membrane type[b]	A201	A901	A901	A901	A901
Anode catalyst loading (mg cm^{-2})	1	1	1	1	1
Cathode catalyst loading (mg cm^{-2})	1	3	3	3	3
Anode catalyst metal loading (wt%)	40	55	55	55	55
Anode fuel flow rate (ml min^{-1})	4	4	1	1	1
Cathode gas flow rate (ml min^{-1})	400	400	100	100	100
Temperature (°C)	50	50	50	60	60
KOH concentration (M)	2	2	2	2	8
Back pressure (psi)	30	30	0	0	0

[a] The MEA structure and operation conditions were used in our previous work [42].
[b] The thickness of Tokuyama A201 and A901 membrane is 28 μm and 10 μm, respectively.

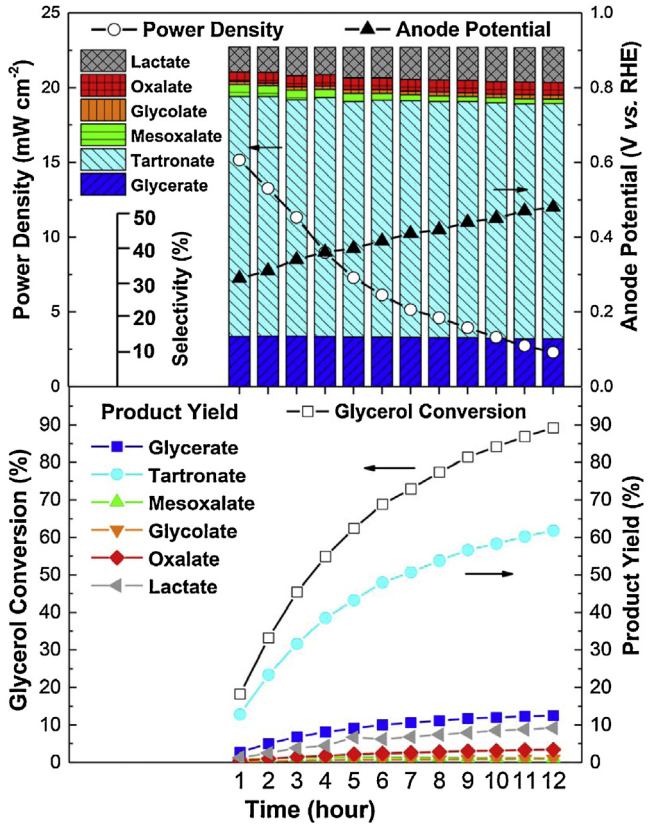

Fig. 4. Electro-catalytic selective oxidation of glycerol on Au/C-NC (55 wt%) in AEM-DGFC under optimized condition for high yield of tartronate. Anode catalyst: Au/C-NC (1 mg_{Au} cm^{-2}); cathode catalyst: Fe-Cu-based catalyst (Acta 4020, 3 mg cm^{-2}), anion exchange membrane (A901, Tokuyama Inc.). Anode fuel: 8.0 M KOH + 1.0 M glycerol, 30 ml, 1.0 ml min^{-1}; Cathode fuel: high purity O_2, 100 ml min^{-1}, ambient pressure. Glycerol:Au = 1:1300 (mol:mol); cell voltage: 0.1 V; cell temperature: 60 °C reaction time: 12 h.

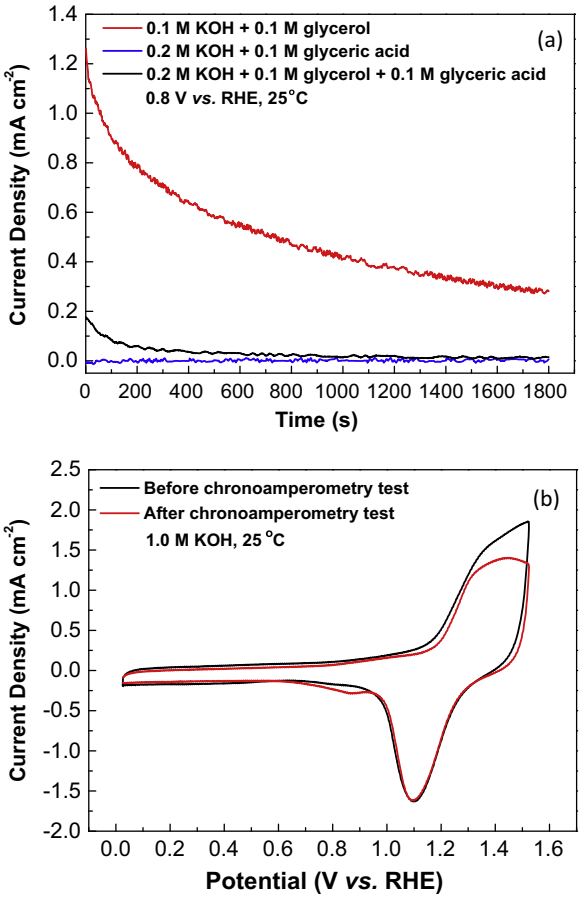

Fig. 5. (a) Influence of glycerate on the chronoameperometric activity of glycerol oxidation on Au/C-NC (55 wt%) at 0.8 V vs. RHE, 25 °C; (b) cyclic voltammograms of Au/C-NC (55 wt%) before and after chronoamperometry (CA) tests with the addition of glyceric acid, used Au/C-NC catalyst was washed with deionized water before the recycle test, 1.0 M KOH, 25 °C.

Fig. 4 also shows that as the reaction was prolonged to 12 h, the glycerol conversion reached 89.2% and the tartronate selectivity only slightly decreased from 70.6% to 69.3%, even though the anode potential of the AEM-DGFC kept increasing from 0.29 V to 0.48 V vs. RHE. This indicates that the final products distribution in bulk electrolyte is governed by both the electrocatalytic reaction at the electrified catalyst–electrolyte interface that can be regulated by the anode potential, and the reactants/reaction intermediates/products diffusion/transport through the catalyst layer. As discussed previously, the MEA structure and reaction conditions of AEM-DGFC were optimized to not only lower the anode potential so as to favor the consecutive oxidation of glycerol to tartronate with less C—C bond cleavage or over-oxidation to mesoxalate, but also facilitate desorption of the intermediates/products off the catalytic active sites and diffusion back to the bulk electrolyte.

The LSVs performed on Au/C-NC in half cell at 60 °C with alkaline electrolytes of glycerate, tartronate, mesoxalate and glycerol are shown in Fig. 2(b). The results showed the electrocatalytic activity sequence of these desorbed glycerate, tartronate and mesoxalate during the glycerol electro-oxidation. Higher anode potential is needed to make them reactive on Au/C-NC electrode. In addition, previous studies by Lamy et al. have found that the glycolate and oxalate cannot be oxidized on Au electrode in alkaline solution in the potential range of 0–1.0 V vs. RHE, which is within the fuel cell anode potential window [49]. For this reason, the products presented in the bulk electrolyte are more difficult to re-adsorb and further oxidize on the Au catalyst as compared with glycerol, resulting in the relatively stable products distribution in the bulk electrolyte and no apparent change in the product selectivity from 1 h to 12 h. In particular, the relatively low activity (onset potential and peak current density) of electro-oxidation "desorbed" tartronate may account for its high selectivity.

However, as glycerol was continuously converted, increasing concentrations of glycerate and tartronate will accumulate in the product mixture solution. It is reported that the adsorption of glycerate or tartronate during the glycerol oxidation could strongly deactivate metal catalysts in the heterogeneous catalysis system, which is attributed to the formation of ketonic species [48,60]. To investigate the influence of the product salts on the rate of glycerol electro-oxidation, equal molar glyceric acid was added to a 0.1 M glycerol solution. Additional KOH was also added to neutralize the glyceric acid in order to maintain a close base to reactant ratio of around 1:1 (mol:mol). Chronoamperometries (CAs) were carried out on Au/C-NC at 0.8 V vs. RHE, where the

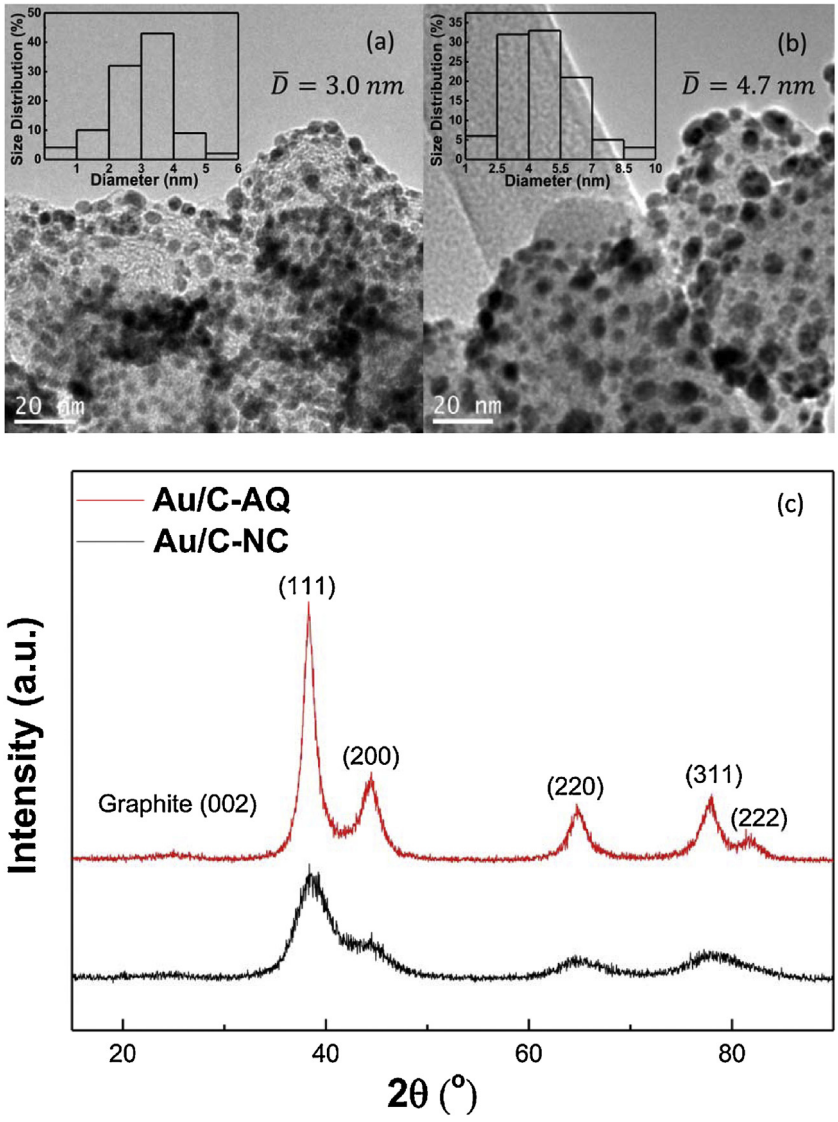

Fig. 6. TEM images and particle size histograms of (a) Au/C-NC, (b) Au/C-AQ; and (c) XRD patterns of Au/C-NC and Au/C-AQ (55 wt% Au loading).

electro-oxidation proceeds slowly so that the mass transport effect is negligible. Fig. 5(a) shows that the oxidation current density of 0.1 M glycerol remains at ca. 0.28 mA cm^{-2} after 1800 s test, while with addition of 0.1 M glycerate, it is significantly lower and drops rapidly to 0.014 mA cm^{-2}. The controlled CA experiment using 0.2 M KOH + 0.1 M glyceric acid showed no current generation on Au/C-NC under the same test conditions, which suggests that the decreased reaction rate is not due to the competitive electro-oxidation of glycerate, but rather due to the inhibitory effect of glycerate. It is worth to mention that the adsorbed glycerate could be washed off with copious deionized water and the active sites of Au/C-NC can be recovered, as evidenced by the similar broad peaks correlated to the reduction of AuO_x during the cyclic voltammetry in 1.0 M KOH before and after CV tests (Fig. 5b). The mechanism of the inhibition of supported metal catalysts by reaction intermediates/products formed in the course of the electro-oxidation of glycerol is still elusive and currently under study in our lab. Nevertheless, the deactivation of Au/C-NC will cause the activity loss of the glycerol electro-oxidation and is responsible for the increasing of the anode potential in AEM-DGFC with the elongated reaction time, as shown in Fig. 4. As a result of anode potential increasing, the selectivites to C—C cleavage products glycolate and oxalate, were increased from 0.8% (after 1 h) to 1.2% (after 12 h) and 2.5% (after 1 h) to 3.8% (after 12 h), respectively.

3.3. *The effect of supported gold nanoparticle synthesis method on glycerol selective electro-oxidation*

The essential role of metal catalysts well recognized in both electrocatalysis and heterogeneous catalysis is to enhance the adsorption, activation and transformation of reactants and reaction/reactive intermediates. Various synthesis routes have been provided to prepare metal catalysts with controlled size, size distribution, structure and morphology, which can drastically affect the activity and selectivity of the heterogeneous catalysts [8,10–12,15,61]. Aiming to study the effect of metal nanoparticle catalyst synthesis methods on the electrocatalytic oxidation of glycerol, we compared electrocatalytic oxidation of glycerol over Au/C catalysts prepared via two synthesis methods, namely nanocapsule method (Au/C-NC) and aqueous-phase reduction method (Au/C-AQ). The Au/C-NC was prepared by reduction of $AuCl_3$ precursor in organic phase solution and C_{18} surfactant oleylamine served as the stabilizer; while the Au/C-AQ was prepared by reduction of $AuCl_3$ in water phase and citrate was used as the stabilizer. TEM images show that the average particle size of Au/C-NC is 3.0 nm (Fig. 6(a)), which is smaller than that of 4.7 nm for Au/C-AQ (Fig. 6(b)). The crystal sizes obtained from (2 2 0) diffraction peaks of XRD are 2.1 nm and 4.6 nm for Au/C-NC and Au/C-AQ, respectively, which agrees well with the TEM characterizations. It is important to note that the size distribution of Au/C-NC ranging from 1–6 nm is also narrower than that of 1–10 nm for Au/C-AQ. The variation of particle sizes and size distributions observed from the two preparation methods can be attributed to the nature of stabilizers and solvent used. Oleylamine with a long-chain primary alkyl-amine can act as electron donor and has strong affinity to Au nanoparticles at the synthesis temperature (80 °C) [62], whereas citrate is purely an electrostatic stabilizer that interacts weakly with the Au nanoparticles [61]. Therefore, the organic phase based nanocapsule method can protect Au particles more effectively from aggregation in the preparation process compared to aqueous phase based method.

The electro-catalytic oxidation of glycerol over Au/C-AQ anode catalyst was performed in AEM-DGFC under the same optimal conditions as Au/C-NC. Fig. 7 shows that glycerol conversion of 95.6% was achieved on Au/C-AQ together with energy generation of 1666 J, which are higher than those for Au/C-NC (89.2% with

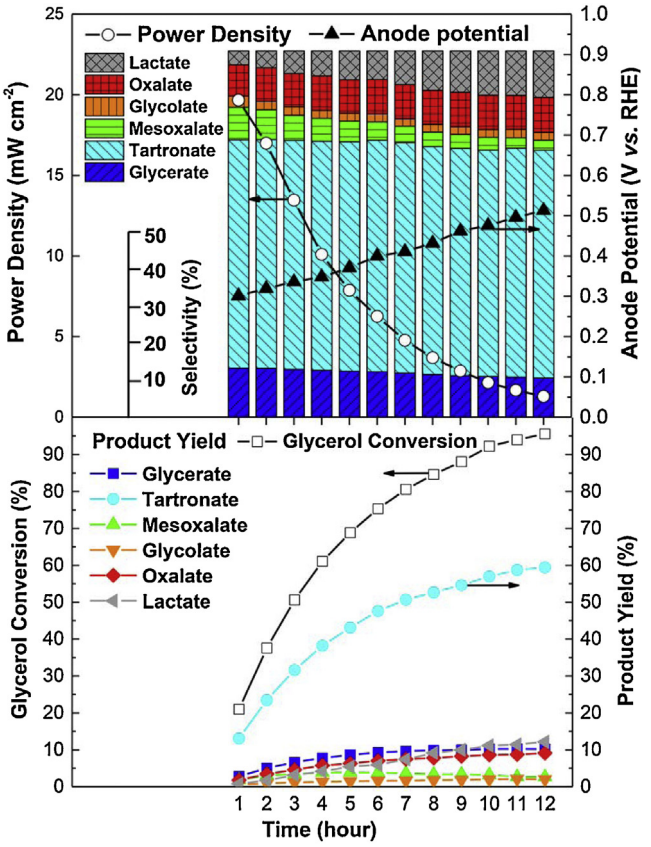

Fig. 7. Electrocatalytic selective oxidation of glycerol on Au/C-AQ (55 wt%) in AEM-DGFC under optimized condition for high yield of tartronate. Anode catalyst: Au/C-AQ (1 mg_{Au} cm^{-2}); cathode catalyst: Fe-Cu-based catalyst (Acta 4020, 3 mg cm^{-2}), anion exchange membrane (A901, Tokuyama Inc.). Anode fuel: 8.0 M KOH + 1.0 M glycerol, 30 ml, 1.0 ml min^{-1}; cathode fuel: high purity O_2, 100 ml min^{-1}, ambient pressure. Glycerol:Au = 1:1300 (mol:mol); cell voltage: 0.1 V; cell temperature: 60 °C reaction time: 12 h.

1527 J of energy generation, Fig. 4). However, the tartronate yield on Au/C-AQ was 61.2% with 10.5% carbon balance, which is very close to 61.8% with 12.5% carbon balance on Au/C-NC as shown in Fig. 4. A possible explanation of different activities may lie in the residual hydrophobic oleylamine on the Au surface [63] limits the accessibility of fresh glycerol across the surfactant ligand layers. The relatively clean surface of Au/C-AQ realized by easy removal of citrate also increases the residence time of reactants/reaction intermediates near the Au/C-AQ active sites and liberates a fraction of active sites for the sequential glycerol electro-oxidation, thus enhancing the rate of further oxidization of the secondary —OH of adsorbed C_3 species to mesoxalate or C—C breakage of adsorbed C_3 species to glycolate and oxalate, following the pathway proposed in our previous publications [28,42,44]. As a result, after the 12 h reaction, the selectivities to mesoxalate from 8.9% to 2.8%, glycolate from 3.0% to 2.1%, oxalate from 8.6% to 9.6% on Au/C-AQ were observed, which are higher than 4.3–1.2% (mesoxalate), 0.8–1.2% (glycolate) and 2.5–3.8% (oxalate) on Au/C-NC. The changed product selectivity during the reaction is perhaps due to the change of Au polarization (anode potential), resulting from the continuous conversion of glycerol and change in product distribution. Furthermore, our results are in good agreement with Hutching's group work [64]: the surfactant bonded to catalyst surface will not apparently change the product yield, while a clean catalyst surface could enhance the reaction rate. Research on preparation of Au-based bimetallic catalysts for electro-oxidation of glycerol in AEMFC is currently underway in our lab.

4. Conclusions

Electrocatalytic selective oxidation of glycerol over Au nanoparticle catalysts to tartronate with a high yield of 61.8% with cogeneration of electrical energy of 1527 J (12 h) has been achieved in a 5 cm^2 AEM-DGFCs. The MEA structure and reaction conditions were found to be able to strongly influence tartronate selectivity during the glycerol electro-oxidation. Rational optimization of the MEA structure, flow rate, oxidation temperature as well as the electrolyte pH could not only tune the anode potentials to <0.45 V in favor of tartronate production, but also improve the mass transport of the reactant and products/intermediates so as to improve the reaction kinetics and desorption rate of produced tartronate off the active sites. The half-cell study on electro-oxidation of C_3 products (glycerate, tartronate and mesoxalate) shows they are less active than glycerol on Au/C, therefore, they are not likely to be further oxidized upon diffusion into the bulk electrolyte. Particularly, the lowest electro-oxidation activity of tartronate may be related with its high selectivity and yield. Furthermore, two Au/C catalysts prepared through the nanocapsule method (Au/C-NC) and aqueous-phase reduction method (Au/C-AQ) were investigated for the electro-catalytic oxidation of glycerol. Au/C-AQ has larger particle size (4.7 nm vs. 3.0 nm for Au/C-NC) and broader size distribution (1–10 nm vs. 1–6 nm for Au/C-NC) due to the different nature of capping agents employed in the synthesis. Under the same electro-oxidation reaction conditions, the conversion of glycerol obtained on Au/C-AQ with cleaner surface was 95.6% in 12 h, which was higher than Au/C-NC of 89.2%, resulting in higher electrical energy generation (1666 J vs. 1527 J). However, the residual surfactants presented on Au/C-NC do not apparently change the product yield, evidenced by the very close tartronate yields with Au/C-AQ (61.2%) and Au/C-NC (61.8%).

Acknowledgements

We gratefully acknowledge the US National Science Foundation (CBET-1159448) for funding and a Michigan Tech REF grant (E49290) for partial support of this work. J. Qi thanks the financial support from the Chinese Scholarship Council.

References

[1] A.J. Ragauskas, C.K. Williams, B.H. Davison, G. Britovsek, J. Cairney, C.A. Eckert, W.J. Frederick, J.P. Hallett, D.J. Leak, C.L. Liotta, J.R. Mielenz, R. Murphy, R. Templer, T. Tschaplinski, Science 311 (2006) 484–489.
[2] C.O. Tuck, E. Pérez, I.T. Horváth, R.A. Sheldon, M. Poliakoff, Science 337 (2012) 695–699.
[3] A. Corma, S. Iborra, A. Velty, Chem. Rev. 107 (2007) 2411–2502.
[4] L. Prati, P. Spontoni, A. Gaiassi, Top. Catal. 52 (2009) 288–296.
[5] B. Katryniok, H. Kimura, E. Skrzynska, J.-S. Girardon, P. Fongarland, M. Capron, R. Ducoulombier, N. Mimura, S. Paul, F. Dumeignil, Green Chem. 13 (2011) 1960–1979.
[6] S. Carrettin, P. McMorn, P. Johnston, K. Griffin, G.J. Hutchings, Chem. Commun. (2002) 696–697.
[7] S. Carrettin, P. McMorn, P. Johnston, K. Griffin, C.J. Kiely, G.J. Hutchings, Phys. Chem. Chem. Phys. 5 (2003) 1329–1336.
[8] F. Porta, L. Prati, J. Catal. 224 (2004) 397–403.
[9] S. Carrettin, P. McMorn, P. Johnston, K. Griffin, C.J. Kiely, G.A. Attard, G.J. Hutchings, Top. Catal. 27 (2004) 131–136.
[10] C.L. Bianchi, P. Canton, N. Dimitratos, F. Porta, L. Prati, Catal. Today 102 (2005) 203–212.
[11] N. Dimitratos, C. Messi, F. Porta, L. Prati, A. Villa, J. Mol. Catal. A: Chem. 256 (2006) 21–28.
[12] W.C. Ketchie, Y.-L. Fang, M.S. Wong, M. Murayama, R.J. Davis, J. Catal. 250 (2007) 94–101.
[13] W.C. Ketchie, M. Murayama, R.J. Davis, Top. Catal. 44 (2007) 307–317.
[14] W.C. Ketchie, M. Murayama, R.J. Davis, J. Catal. 250 (2007) 264–273.
[15] N. Dimitratos, J.A. Lopez-Sanchez, J.M. Anthonykutty, G. Brett, A.F. Carley, R.C. Tiruvalam, A.A. Herzing, C.J. Kiely, D.W. Knight, G.J. Hutchings, Phys. Chem. Chem. Phys. 11 (2009) 4952–4961.
[16] N. Dimitratos, A. Villa, L. Prati, Catal. Lett. 133 (2009) 334–340.
[17] B.N. Zope, S.E. Davis, R.J. Davis, Top. Catal. 55 (2012) 24–32.
[18] A. Villa, C.E. Chan-Thaw, L. Prati, Appl. Catal. B: Environ. 96 (2010) 541–547.
[19] B.N. Zope, R.J. Davis, Top. Catal. 52 (2009) 269–277.
[20] H. Kimura, T. Imanaka, Y. Yokota, (Kao Corp.), JP 199395253, 1994.
[21] A. Villa, D. Wang, G.M. Veith, L. Prati, J. Catal. 292 (2012) 73–80.
[22] D.Z. Jeffery, G.A. Camara, Electrochem. Commun. 12 (2010) 1129–1132.
[23] Y. Kwon, M.T.M. Koper, Anal. Chem. 82 (2010) 5420–5424.
[24] M. Simoes, S. Baranton, C. Coutanceau, Appl. Catal. B: Environ. 93 (2010) 354–362.
[25] J.F. Gomes, G. Tremiliosi-Filho, Electrocatalysis 2 (2011) 96–105.
[26] Y. Kwon, K.J.P. Schouten, M.T.M. Koper, ChemCatChem 3 (2011) 1176–1185.
[27] Z. Zhang, L. Xin, W. Li, Appl. Catal. B: Environ. 119 (2012) 40–48.
[28] Z. Zhang, L. Xin, J. Qi, D.J. Chadderdon, K. Sun, K.M. Warsko, W. Li, Appl. Catal. B: Environ. 147 (2014) 871–878.
[29] L. Roquet, E.M. Belgsir, J.M. Léger, C. Lamy, Electrochim. Acta 39 (1994) 2387–2394.
[30] M. Simoes, S. Baranton, C. Coutanceau, Appl. Catal. B: Environ. 110 (2011) 40–49.
[31] K. Matsuoka, Y. Iriyama, T. Abe, M. Matsuoka, Z. Ogumi, J. Power Sources 150 (2005) 27–31.
[32] E. Antolini, Energy Environ. Sci. 2 (2009) 915–931.
[33] V. Bambagioni, C. Bianchini, A. Marchionni, J. Filippi, F. Vizza, J. Teddy, P. Serp, M. Zhiani, J. Power Sources 190 (2009) 241–251.
[34] C. Bianchini, P.K. Shen, Chem. Rev. 109 (2009) 4183–4206.
[35] V. Bambagioni, M. Bevilacqua, J. Filippi, A. Marchionni, S. Moneti, F. Vizza, C. Bianchini, Chim. Oggi 28 (2010) VII–X.
[36] V. Bambagioni, M. Bevilacqua, C. Bianchini, J. Filippi, A. Lavacchi, A. Marchionni, F. Vizza, P.K. Shen, ChemSusChem 3 (2010) 851–855.
[37] M. Simões, S. Baranton, C. Coutanceau, ChemSusChem 5 (2012) 2106–2124.
[38] Z. Zhang, L. Xin, W. Li, Int. J. Hydrogen Energy 37 (2012) 9393–9401.
[39] J. Qi, L. Xin, Z. Zhang, K. Sun, H. He, F. Wang, D. Chadderdon, Y. Qiu, C. Liang, W. Li, Green Chem. 15 (2013) 1133–1137.
[40] A. Marchionni, M. Bevilacqua, C. Bianchini, Y.-X. Chen, J. Filippi, P. Fornasiero, A. Lavacchi, H. Miller, L. Wang, F. Vizza, ChemSusChem 6 (2013) 518–528.
[41] M. Mougenot, A. Caillard, M. Simoes, S. Baranton, C. Coutanceau, P. Brault, Appl. Catal. B: Environ. 107 (2011) 372–379.
[42] L. Xin, Z. Zhang, Z. Wang, W. Li, ChemCatChem 4 (2012) 1105–1114.
[43] A. Ilie, M. Simoes, S. Baranton, C. Coutanceau, S. Martemianov, J. Power Sources 196 (2011) 4965–4971.
[44] Z. Zhang, L. Xin, J. Qi, Z. Wang, W. Li, Green Chem. 14 (2012) 2150–2152.
[45] B.N. Zope, D.D. Hibbitts, M. Neurock, R.J. Davis, Science 330 (2010) 74–78.
[46] D.D. Perrin, B. Dempsey, E.P. Serjeant, pK_a Prediction for Organic Acids and Bases, Chapman and Hall, London, 1981.
[47] Z. Zhang, L. Xin, J. Qi, D.J. Chadderdon, W. Li, Appl. Catal. B: Environ. 136-137 (2013) 29–39.
[48] B.N. Zope, R.J. Davis, Green Chem. 13 (2011) 3484–3491.
[49] B. Beden, I. Çetin, A. Kahyaoglu, D. Takky, C. Lamy, J. Catal. 104 (1987) 37–46.
[50] L. Xin, Z. Zhang, J. Qi, D. Chadderdon, W. Li, Appl. Catal. B: Environ. 125 (2012) 85–94.
[51] Y. Kwon, S.C.S. Lai, P. Rodriguez, M.T.M. Koper, J. Am. Chem. Soc. 133 (2011) 6914–6917.
[52] M.L. Avramov-Ivić, J.-M. Leger, C. Lamy, V.D. Jovic, S.D. Petrovic, J. Electroanal. Chem. 308 (1991) 309.
[53] B. Braunchweig, D. Hibbitts, M. Neurock, A. Wieckowski, Catal. Today 202 (2013) 197–209.
[54] S.C.S. Lai, S.E.F. Kleijn, F.T.Z. Öztürk, V.C. van Rees Vellinga, J. Koning, P. Rodriguez, M.T.M. Koper, Catal. Today 154 (2010) 92–104.
[55] C.A. Gandolfi, L. Cotini, M. Mantovanini, G. Caselli, G. Clavenna, C. Omini, (DompeFarmaceutici S.P.A), WO 1994010127, 1994.
[56] S.E. Solovyov, (Multisorb Technologies Inc.), WO 2007013978, 2007.
[57] T. Powers, (Maultisorb Technologies Inc.), WO 2006016916, 2006.
[58] T. Powers, (Maultisorb Technologies Inc.), WO 2005040304, 2005.
[59] P.M. Bizot, B.R. Bailey, P.D. Hicks, (Nalco Chemical Company), WO 1998016475, 1998.
[60] N. Worz, A. Brandner, P. Claus, J. Phys. Chem. C 114 (2009) 1164–1172.
[61] A. Villa, D. Wang, D.S. Su, L. Prati, ChemCatChem 1 (2009) 510–514.
[62] S. Mourdikoudis, L.M. Liz-Marzán, Chem. Mater. 25 (2013) 1465–1476.
[63] Z. Zhang, L. Xin, K. Sun, W. Li, Int. J. Hydrogen Energy 36 (2011) 12686–12697.
[64] J.A. Lopez-Sanchez, N. Dimitratos, C. Hammond, G.L. Brett, L. Kesavan, S. White, P. Miedziak, R. Tiruvalam, R.L. Jenkins, A.F. Carley, D. Knight, C.J. Kiely, G.J. Hutchings, Nature Chem. 3 (2011) 551–556.